Cancer Therapy

Deutsche Ausgabe: DOI: 10.1002/ange.201411417
Internationale Ausgabe: DOI: 10.1002/anie.201411417

A Smart DNAzyme–MnO_2 Nanosystem for Efficient Gene Silencing**

*Huanhuan Fan, Zilong Zhao, Guobei Yan, Xiaobing Zhang, Chao Yang, Hongmin Meng, Zhuo Chen, Hui Liu, and Weihong Tan**

Dedicated to Professor Ru-Qin Yu on the occasion of his 80th birthday

Abstract: *DNAzymes hold promise for gene-silencing therapy, but the lack of sufficient cofactors in the cell cytoplasm, poor membrane permeability, and poor biostability have limited the use of DNAzymes in therapeutics. We report a DNAzyme–MnO_2 nanosystem for gene-silencing therapy. MnO_2 nanosheets adsorb chlorin e6-labelled DNAzymes (Ce6), protect them from enzymatic digestion, and efficiently deliver them into cells. The nanosystem can also inhibit $^1O_2$ generation by Ce6 in the circulatory system. In the presence of intracellular glutathione (GSH), MnO_2 is reduced to Mn^{2+} ions, which serve as cofactors of 10–23 DNAzyme for gene silencing. The release of Ce6 generates $^1O_2$ for more efficient photodynamic therapy. The Mn^{2+} ions also enhance magnetic resonance contrast, providing GSH-activated magnetic resonance imaging (MRI) of tumor cells. The integration of fluorescence recovery and MRI activation provides fluorescence/MRI bimodality for monitoring the delivery of DNAzymes.*

DNAzymes, generated through in vitro selection processes, are single-stranded DNA (ssDNA) catalysts that can catalyze a wide variety of reactions, such as RNA or DNA cleavage and ligation or DNA phosphorylation.[1] Based on specific cofactor dependence and potent catalytic ability, especially nucleic acid cleavage,[2] DNAzymes have been extensively used to develop highly sensitive and specific sensing platforms for metal ions, small molecules, and biomacromolecules by integrating various signal transduction mechanisms, such as fluorescence,[3] colorimetry,[4] electrochemistry,[5] and electrochemiluminescence.[6] However, in spite of their multiple strong enzymatic turnover properties and promise for selective gene silencing, few reports have addressed the potential application of RNA-cleaving DNAzymes as therapeutic gene-silencing agents,[7] the main barrier being the need for a high cofactor concentration to maintain catalytic activity. For example, the most widely investigated DNAzyme for RNA cleavage is 10–23 DNAzyme,[8] which requires at least 5 mM of Mg^{2+} ions to form the catalytic domain and efficiently cleave the substrate. However, with the concentration of free Mg^{2+} ions in animal cells ranging from 0.2 to 2 mM,[9] the formation of the 10–23 DNAzyme catalytic domain cannot be facilitated, thus resulting in low intracellular catalytic activity. Its poor cell penetration and equally poor stability in biofluids also limit the application of 10–23 DNAzyme in gene silencing.[10] Therefore, the development of a smart carrier that can enhance the cellular uptake of DNAzymes, protect DNAzymes from endogenous nuclease digestion, and self-generate cofactors in situ in the cytoplasm for catalysis is highly desired.

Ultrathin MnO_2 nanosheets, typical electrode materials for energy storage, have attracted extensive attention in bioanalysis, cell imaging, and drug delivery as a result of their appealing physicochemical properties.[11] First, MnO_2 nanosheets can strongly adsorb ssDNA by physisorption between nucleobases and MnO_2 nanosheets, which can facilitate the endocytosis of ssDNA. Second, MnO_2 nanosheets have an intense and broad optical absorption spectrum ($\lambda \approx 200$–600 nm), making them an efficient broad-spectrum fluorescence quencher. Third, MnO_2 nanosheets can be reduced to Mn^{2+} ions by intracellular glutathione (GSH). The produced Mn^{2+} ions can then be used as efficient cofactors of 10–23 DNAzyme for gene silencing.[12] Meanwhile, the reduction of MnO_2 can also provide activatable magnetic resonance and fluorescence signaling to monitor the efficacy of delivery. Therefore, MnO_2 nanosheets provide a potent nanocarrier for delivering DNAzyme into cells for gene silencing and simultaneous monitoring of delivery efficacy through cellular imaging.

In this work, a DNAzyme–MnO_2 nanosystem was prepared by the physisorption of nucleobases on MnO_2 nanosheets for efficient gene-silencing therapy, as shown in Scheme 1. In this design, Ce6-labelled DNAzyme acts as an agent for gene silencing, photodynamic therapy, and fluorescence imaging. MnO_2 nanosheets have multiple roles, serving as the nanocarrier for the DNAzyme, as a potential provider of cofactor (Mn^{2+}) for 10–23 DNAzyme, as a quencher for singlet oxygen generation and fluorescence from Ce6, and as an activatable MRI contrast agent. In the Ce6–DNAzyme–MnO_2 nanosystem, DNAzyme is protected from enzymatic

[*] H. Fan,[+] Dr. Z. Zhao,[+] G. Yan, Prof. X. Zhang, Dr. C. Yang, H. Meng, Z. Chen, H. Liu, Prof. W. Tan
Molecular Science and Biomedicine Laboratory
State Key Laboratory of Chemo/Bio-Sensing and Chemometrics
College of Chemistry and Chemical Engineering, College of Biology
Collaborative Innovation Center for Chemistry and Molecular Medicine, Hunan University, Changsha, 410082 (China)
E-mail: tan@chem.ufl.edu

[+] These authors contributed equally to this work.

[**] This work was supported by the National Key Scientific Program of China (2011CB911000), the National Key Basic Research Program of China (No. 2013CB932702), the NSFC (Grants 21325520, 21327009, 21405041, J1210040, 21177036), the Foundation for Innovative Research Groups of NSFC (Grant 21221003), the National Instrumentation Program (2011YQ030124), and the Hunan Provincial Natural Science Foundation (Grant 11JJ1002).

Supporting information for this article is available on the WWW under http://dx.doi.org/10.1002/anie.201411417.

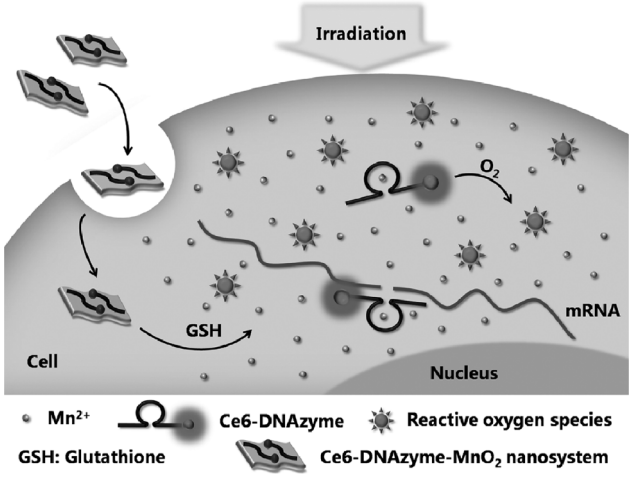

Scheme 1. Activated mechanism of the Ce6–DNAzyme–MnO_2 nanosystem for gene silencing and PDT. The nanosheet can adsorb and efficiently deliver DNAzymes into cells and protect them from enzymatic digestion. In the presence of cellular GSH, the MnO_2 nanosheet is reduced to Mn^{2+} ions, and DNAzyme is freed for efficient gene silencing with in situ generated Mn^{2+} as the cofactor. Ce6 is also released to generate singlet oxygen for PDT after irradiation.

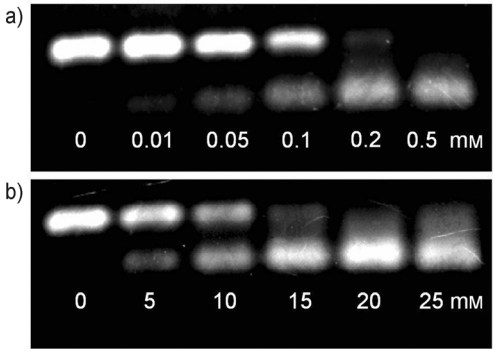

Figure 1. Agarose gel electrophoresis analysis of DNAzyme catalytic efficiency with a) Mn^{2+} and b) Mg^{2+} as the cofactors. The substrate and DNAzyme concentrations were both 2.5 μM. Cleavage experiments were carried out at 37 °C for 60 min.

digestion and can be efficiently delivered into the cytoplasm. Once endocytosed, the nanosystem is decomposed by the reduction of MnO_2 nanosheets by intracellular GSH, generating a large amount of Mn^{2+} ions as cofactors for 10–23 DNAzyme cleavage to target RNA. The therapeutic efficacy can be further enhanced by the photodynamic effect of Ce6. Meanwhile, fluorescence recovery and activation of an MRI contrast agent, accompanied by the dissolution of MnO_2 nanosheets, can provide a fluorescence/MRI bimodal signal for monitoring the efficacy of delivery.

To construct the DNAzyme–MnO_2 nanosystem, MnO_2 nanosheets were prepared by ultrasonicating bulk MnO_2, which was synthesized using H_2O_2 to oxidize $MnCl_2$ in the presence of tetramethylammonium hydroxide.[13] The product was identified by X-ray photoelectron spectroscopy (see Figure S1 in the Supporting Information). The results from transmission electron microscopy (TEM) and atomic force microscopy (AFM) indicated that the as-prepared MnO_2 has a sheet-like structure about 1.5 nm in thickness (Figure S2). The as-prepared MnO_2 had an intense UV/Vis absorption with a band centered at $\lambda = 360$ nm in the absorption spectrum. Based on the high efficacy and the potential flexibility in the design of recognition arms,[8b,14] 10–23 DNAzyme (Table S1) was chosen as a model DNAzyme to cleave the human early growth response-1 (EGR-1) gene, which has been reported to regulate breast cancer cell proliferation, migration, chemoinvasion, and xenograft growth in nude mice.[15]

To investigate whether the produced Mn^{2+} ions from the reduction of MnO_2 nanosheets could act as cofactors for 10–23 DNAzyme, the effect of Mn^{2+} on the catalytic activity of DNAzyme for RNA cleavage was analyzed by agar electrophoresis. It can be seen in Figure 1 that 0.2 mM of Mn^{2+} ions could trigger 10–23 DNAzyme to completely cleave the substrate within 60 min. However, under the same conditions, a concentration of 15 mM was necessary for Mg^{2+} ions, indicating that the Mn^{2+} ion was the more efficient cofactor. The effect of incubation time on the efficiency of RNA cleavage of 10–23 DNAzyme was further investigated by agar electrophoresis and fluorescence analysis. It was found that the effect of Mn^{2+} ions on the cleavage efficiency was proportional to incubation time and that 2.5 μM of substrate mRNA could be cleaved completely by 2.5 μM of DNAzyme in the presence of 500 μM of Mn^{2+} ions at 37 °C within 60 min (Figure S3a and S3b). These results demonstrate that the MnO_2 nanosheet can be an efficient procofactor for 10–23 DNAzyme for gene silencing.

The excellent fluorescence quenching ability of MnO_2 nanosheets made it possible to test the amount of 10–23 DNAzyme adsorbed on the MnO_2 nanosheets by fluorescence analysis. Accordingly, when 100 nM of carboxyfluorescein-labelled DNAzyme (FAM–DNAzyme) was mixed with different concentrations of MnO_2 nanosheets, it was found that the fluorescence of FAM was gradually decreased with the increasing concentration of introduced nanosheets, until it was totally quenched at a concentration of 26. 81 μg mL^{-1} (Figure S4). At this concentration, the amount of adsorbed DNAzyme on 1 μg of the as-prepared MnO_2 nanosheets was calculated to be about 3.26 pmol.

The instability of DNAzymes in biofluids has been a factor limiting their clinical application. To identify whether the noncovalent adsorption of DNAzyme onto MnO_2 nanosheets could defend against enzymatic digestion, the fluorescence change of free FAM-labelled ssDNA and ssDNA–MnO_2 nanocomplexes, respectively, in the presence of deoxyribonuclease I (DNase I) was investigated. It can be seen in Figure S5 that the free molecular beacon (MB), specifically FAM, was gradually cleaved by DNase I. However, even when DNAzyme–MnO_2 or MB–MnO_2 nanocomplexes were treated with 1 U mL^{-1} DNase I (significantly greater than what would be found in the cellular environment) for one hour, no obvious fluorescence changes were detected. These experimental results demonstrate that DNAzyme can be protected from DNase I cleavage after adsorption onto the MnO_2 nanosheets.

Reduced substance-activated fluorescence enhancement and singlet oxygen generation from Ce6 were then investigated by fluorescence analysis and using the reagent singlet oxygen sensor green (SOSG), respectively. As shown in Figure S6, the Ce6–DNAzyme–MnO_2 solution presented a low fluorescence signal after irradiation with light at $\lambda =$ 404 nm. However, an 8.1-fold and 22-fold enhancement of Ce6 fluorescence and a 2.8-fold and 5.2-fold enhancement of SOSG fluorescence was detected in the presence of 0.25 mM and 0.5 mM of DL-dithiothreitol (DTT), respectively. These results indicate that MnO_2 nanosheets can efficiently quench fluorescence and inhibit singlet oxygen generation from Ce6 to decrease phototoxicity during circulation. Additionally, the results show that the introduction of a reduced substance (e.g. GSH) can trigger the disintegration of MnO_2 nanosheets, in turn causing the recovery of fluorescence and singlet oxygen generation of Ce6 for cellular imaging and photodynamic therapy (PDT).

Next, the efficacy of the delivery of MnO_2 nanosheets was examined, comparing the internalization of the Ce6–DNAzyme–MnO_2 nanosystem and that of free DNAzyme in MCF-7 breast-cancer cells. As shown in confocal laser scanning microscopy analysis (Figure 2), MCF-7 cells treated

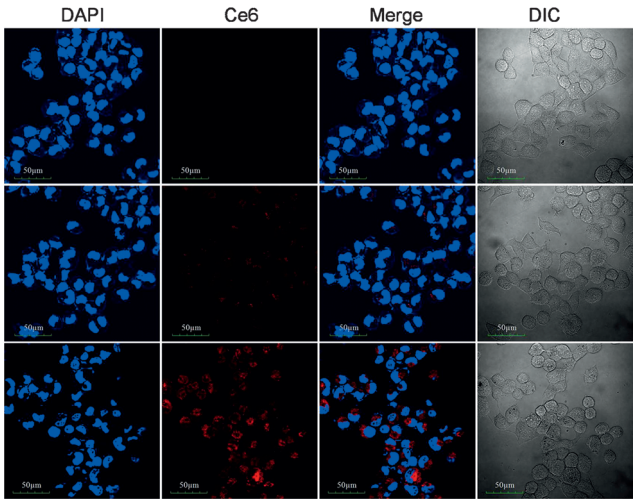

Figure 2. Confocal fluorescence images of MCF-7 cells without treatment (upper) and with treatment with Ce6–DNAzyme (middle) and the Ce6–DNAzyme–MnO_2 nanosystem (lower). The total cellular DNA was stained with DAPI. In all images scale bars = 50 μm. Merge = overlay of Ce6 and DAPI channels. DIC = differential interference contrast image.

with the Ce6–DNAzyme–MnO_2 nanosystem presented stronger fluorescence signals in the cytoplasm than those treated with free Ce6–DNAzyme, indicating that the MnO_2 nanosheets could enhance the cellular uptake of DNAzyme. Internalization was also investigated by using flow cytometry. After the fluorescence signal on the cell surface was removed, cells incubated with the Ce6–DNAzyme–MnO_2 nanosystem showed significantly higher fluorescence intensity than those treated with free Ce6–DNAzyme, in good agreement with the results of confocal microscopy (Figure S7). These data suggest that the MnO_2 nanosheets can efficiently deliver Ce6-labelled DNAzymes into cells for therapeutic applications.

The intracellular manganese contents in MCF-7 cells after treatment with MnO_2 nanosheets was also analyzed by inductively coupled plasma optical emission spectrometry (ICP–OES). The manganese concentrations in MCF-7 cells incubated with 21.8 μg mL^{-1} and 43.6 μg mL^{-1} MnO_2 nanosheets were 0.08 pg/cell and 0.21 pg/cell, respectively (Figure S8). Given the small volume of a single cell (the average diameter of a MCF-7 cell detached by trypsin is about 25 μm), MnO_2 nanosheets can provide a sufficient number of Mn^{2+} ions to activate 10–23 DNAzyme after reduction. Compared with MnO_2 nanosheets, the Mn^{2+} product also has a higher longitudinal relaxivity r_1 and transverse relaxivity r_2 than MnO_2 nanosheets (Figure 3a,c and b,d). After treat-

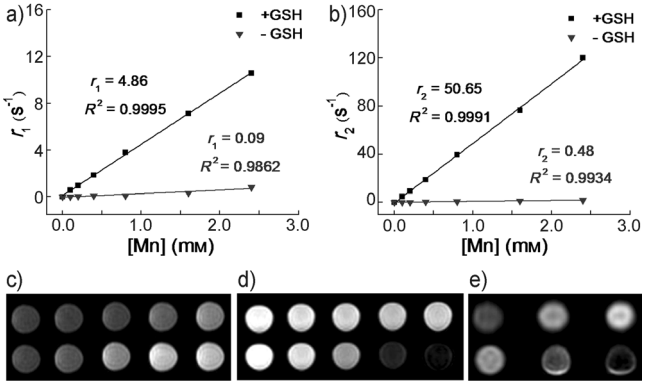

Figure 3. Plots of a) r_1 and b) r_2 versus [Mn] for a MnO_2 nanosheet solution (▼) and a MnO_2 nanosheet solution treated with GSH (■). c) T_1-weighted and d) T_2-weighted MRI results obtained from (a) and (b). Left to right: [Mn] = 0, 0.2, 0.4, 0.8, and 1.6 mM. The top and bottom rows in (c) and (d) correspond to MnO2 nanosheets in the absence and presence of GSH, respectively. e) T_1-weighted (upper) and T_2-weighted (lower) images of MCF-7 cells treated with MnO_2 nanosheets at concentrations of 0, 21.8, and 43.6 μg mL^{-1}.

ment with the nanosystem, MCF-7 cells presented enhanced magnetic resonance contrast (Figure 3e), providing GSH-activated MRI for tumor-cell imaging. Thus, the integration of fluorescence recovery and MRI activation, accompanied and promoted by the disintegration of MnO_2 nanosheets, provides fluorescence/MRI bimodality for monitoring the delivery efficacy of DNAzymes.

To identify whether EGR-1 mRNA was really cleaved by the nanosystem, we first analyzed the expression of EGR-1 mRNA in MCF-7 cells treated with or without the DNAzyme–MnO_2 nanosystem by quantitative real-time PCR analysis. As shown in Figure 4a, mRNA level of EGR-1 was inhibited by 60% after treatment with the nanosystem containing 5 μM of DNAzyme (DNAzyme–MnO_2). However, equivalent quantities of free DNAzyme, the inactive control DNA, and the control DNA–MnO_2 nanocomplex had little effect on the expression of EGR-1 mRNA. The inhibitory effect of the nanosystem on EGR-1 protein expression was further studied. It could be clearly seen in western blot analysis that EGR-1 protein expression decreased in cells

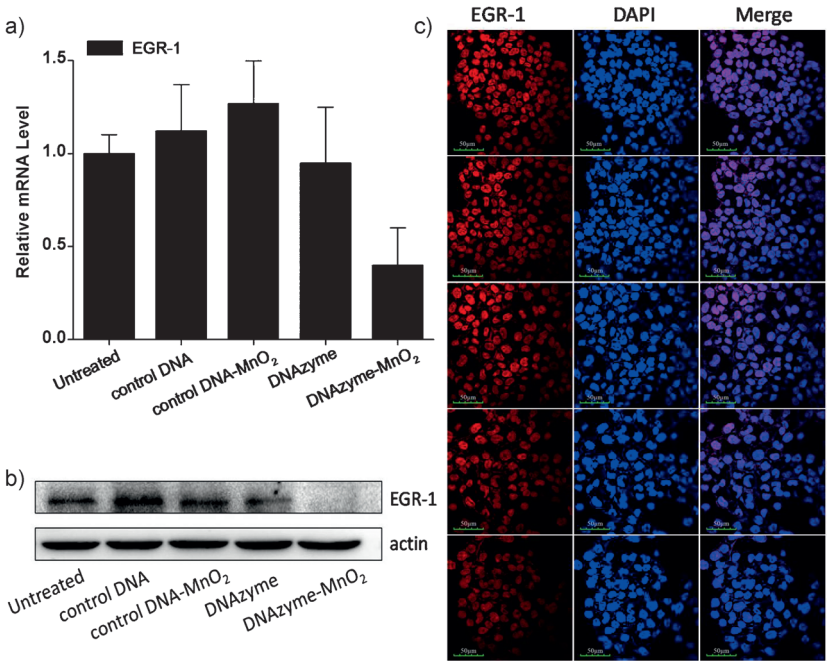

Figure 4. a) Reverse transcriptase quantitative PCR analysis of EGR-1 expression in MCF-7 cells treated with 5 μM control DNA, the control DNA–MnO_2 nanosystem, 5 μM DNAzyme, and the DNAzyme–MnO_2 nanosystem. b) Western blot analysis with antibodies against EGR-1 and β-actin. Samples were treated with the systems used in (a). c) Immunofluorescence analysis with antibodies against EGR-1. MCF-7 cells were treated with the same systems as in (a). Samples from top to bottom: untreated cells, cells treated with control DNA, the control DNA–MnO_2, the DNAzyme, and with the DNAzyme–MnO_2 nanosystem. Merge = overlay of EGR-1 and DAPI channels. Concentration of MnO_2 nanosheets = 40.2 μg mL^{-1}. Scale bars in all images in (c) = 50μm.

treated with the DNAzyme–MnO_2 nanosystem in contrast to cells treated with free DNAzyme, the control DNA, and the control DNA–MnO_2 nanocomplex (Figure 4b). The inhibitory effect of the nanosystem on protein expression was also identified by immunofluorescence assays. The relatively small knockdown in EGR-1 detected in the immunofluorescence results may have to do with the specificity of the antibody in our experiments. As shown in Figure 4c, cells treated with the DNAzyme–MnO_2 nanosystem exhibited weaker fluorescence signals in the nucleus than those treated with free DNAzyme, the control DNA, and the control DNA–MnO_2 nanocomplex. The results demonstrated strongly that the DNAzyme–MnO_2 nanosystem could efficiently cleave its target mRNA and decrease the expression of the translated product of the target mRNA, providing a powerful gene-silencing tool.

To investigate the gene silencing therapeutic efficacy of the DNAzyme–MnO_2 nanosystem, the proliferation of MCF-7 cells treated with a nanosystem containing different concentrations of DNAzymes was evaluated using an MTS assay and a soft-agar colony assay (MTS = 3-(4,5-dimethylthiazol-2-yl)-5-(3-carboxymethoxyphenyl)-2-(4-sulfophenyl)-2H-tetrazolium). As shown in Figure 5a, cell proliferation gradually decreased with increasing concentration of DNAzyme. A nanosystem containing 5 μM of DNAzyme could induce 73% of cell antiproliferation. However, free DNAzyme at 5 μM caused only 15% of cell antiproliferation. The potent antiproliferation of the nanosystem on MCF-7 cells was further identified using a soft-agar colony assay, in which the number and volume of cell colonies treated with nanosystem were clearly fewer than those of cell colonies treated with free DNAzyme. Additionally, only 18% of antiproliferation was detected when MCF-7 cells were treated with DNAzyme–graphene oxide (DNAzyme–GO) nanocomplexes containing 5 μM of DNAzyme (Figure S10), which was slightly higher than the antiproliferation efficacy of free DNAzyme and much lower than that of DNAzyme–MnO_2 nanocomplexes. The difference in antiproliferation efficacy between DNAzyme–MnO_2 and DNAzyme–GO could be because a large amount of Mn^{2+} ions is generated after DNAzyme–MnO_2 is internalized into cells to act as efficient cofactors to facilitate 10–23 DNAzyme RNA cleavage. These results show that the MnO_2 nanosheet is both a potent delivery tool and an efficient cofactor provider to facilitate DNAzyme-based gene-silencing therapy.

Based on the fact that DNA is easy to synthesize and modify with other therapeutic agents, photosensitizer Ce6 was introduced to enhance the therapeutic efficacy of the DNAzyme–MnO_2 nanosystem. The synergistic therapeutic efficacy of DNAzyme-based gene silencing and PDT of the Ce6–DNAzyme–MnO_2 nanosystem was further investigated by using an MTS assay. As shown in Figure 6, under the same conditions the DNAzyme–MnO_2 nanosystem and the Ce6-control DNA–MnO_2 nanocomplex inhibited the proliferation of MCF-7 cells by 35% and 54%, respectively, while the Ce6–DNAzyme–MnO_2 nanosystem inhibited cell proliferation by 78%, demonstrating a remarkably improved and synergistic therapeutic effect. In contrast, an equivalent

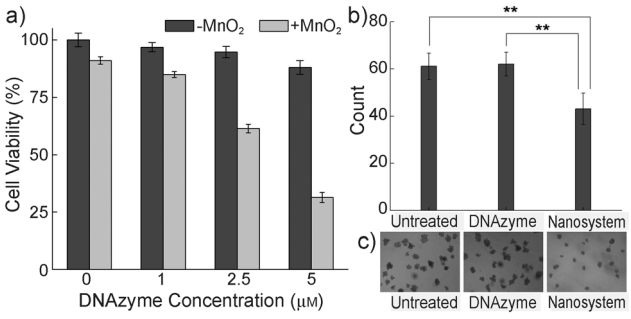

Figure 5. a) Gene-silencing therapy with the DNAzyme–MnO_2 nanosystem, in which MCF-7 cells were treated with different concentrations of DNAzyme and the DNAzyme–MnO_2 nanosystem. b) Statistical analysis of results from the soft-agar colony assay. MCF-7 cells were treated with MnO_2 nanosheets, 2.5 μM DNAzyme, and the DNAzyme–MnO_2 nanosystem at [DNAzyme] = 2.5 μM. *P* values were calculated by *t*-test. ** $P < 0.01$. c) Confocal images of samples from (b). The concentration of MnO_2 nanosheets was 40.2 μg mL^{-1}.

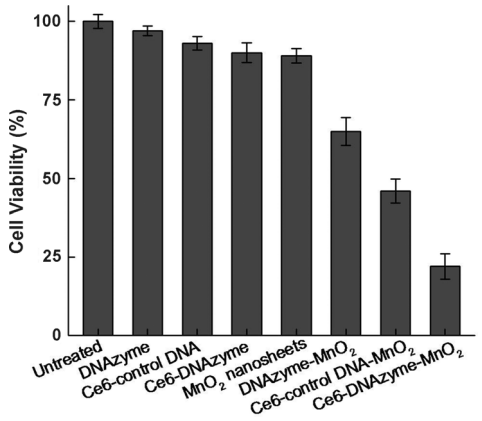

Figure 6. Antiproliferation effects of gene silencing, PDT, and simultaneous gene silencing/PDT. MCF-7 cells were treated with different samples as indicated. The concentrations of ssDNA and MnO_2 nanosheets were 2.5 μM and 40.2 $\mu g\,mL^{-1}$, respectively.

free Ce6–DNAzyme concentration only inhibited 11 % of cell growth, again indicating that the MnO_2 nanosheet is a potent delivery tool for DNAzyme-based therapeutic reagents. Moreover, MnO_2 nanosheets were found to be inefficient for the inhibition of cell growth at a 60 $\mu g\,mL^{-1}$ concentration (Figure S9). These data suggest that the smart DNAzyme–MnO_2 nanosystem inhibits proliferation of cancer cells with excellent biocompatibility.

In summary, we have developed a smart DNAzyme–MnO_2 nanosystem for gene-silencing therapy and cellular imaging. In this nanosystem, we prepared a smart carrier for DNAzymes in which MnO_2 nanosheets are able to enhance cellular uptake of DNAzymes, protect them from endogenous nuclease digestion, and self-generate cofactors (Mn^{2+} ions) in situ in the cytoplasm to maintain the catalytic activity of 10-23 DNAzyme for RNA cleavage. This design affords a nanoplatform for efficient DNAzyme-based gene-silencing therapy. By modifying the DNAzyme with photosensitizer Ce6, a Ce6–DNAzyme–MnO_2 nanosystem was further constructed for bimodal cancer therapy (gene silencing and PDT), with a remarkably improved therapeutic effect over that of gene-silencing therapy or PDT alone. Therefore, this smart DNAzyme–MnO_2 nanosystem shows high promise as a future multifunctional treatment tool for simultaneous therapies and monitoring for various types of cancers.

Keywords: DNAzyme · gene silencing · manganese · nanotechnology · photodynamic therapy

How to cite: *Angew. Chem. Int. Ed.* **2015**, *54*, 4801–4805
Angew. Chem. **2015**, *127*, 4883–4887

[1] J. Liu, Z. Cao, Y. Lu, *Chem. Rev.* **2009**, *109*, 1948–1998.
[2] a) R. R. Breaker, G. F. Joyce, *Chem. Biol.* **1994**, *1*, 223–229; b) S. K. Silverman, *Acc. Chem. Res.* **2009**, *42*, 1521–1531.
[3] a) J. Liu, Y. Lu, *J. Am. Chem. Soc.* **2007**, *129*, 9838–9839; b) Y. Xiang, A. Tong, Y. Lu, *J. Am. Chem. Soc.* **2009**, *131*, 15352–15357; c) P. Wu, K. Hwang, T. Lan, Y. Lu, *J. Am. Chem. Soc.* **2013**, *135*, 5254–5257; d) H. Wang, Y. Kim, H. Liu, Z. Zhu, S. Bamrungsap, W. Tan, *J. Am. Chem. Soc.* **2009**, *131*, 8221–8226; e) L. Lu, X. Zhang, R. Kong, B. Yang, W. Tan, *J. Am. Chem. Soc.* **2011**, *133*, 11686–11691; f) L. Qiu, T. Zhang, J. Jiang, C. Wu, G. Zhu, M. You, X. Chen, L. Zhang, C. Cui, R. Yu, W. Tan, *J. Am. Chem. Soc.* **2014**, *136*, 13090–13093.
[4] a) J. Liu, Y. Lu, *J. Am. Chem. Soc.* **2003**, *125*, 6642–6643; b) J. Liu, Y. Lu, *J. Am. Chem. Soc.* **2005**, *127*, 12677–12683; c) M. Deng, D. Zhang, Y. Zhou, X. Zhou, *J. Am. Chem. Soc.* **2008**, *130*, 13095–13102; d) B. Yin, B. Ye, W. Tan, H. Wang, C. Xie, *J. Am. Chem. Soc.* **2009**, *131*, 14624–14625.
[5] a) Y. Xiao, A. A. Rowe, K. W. Plaxco, *J. Am. Chem. Soc.* **2007**, *129*, 262–263; b) L. Shen, Z. Chen, Y. Li, S. He, S. Xie, X. Xu, Z. Liang, X. Meng, Q. Li, Z. Zhu, M. Li, X. Le, Y. Shao, *Anal. Chem.* **2008**, *80*, 6323–6328.
[6] X. Zhu, Z. Lin, L. Chen, B. Qiu, G. Chen, *Chem. Commun.* **2009**, 6050–6052.
[7] a) C. R. Dass, P. F. Choong, L. M. Khachigian, *Mol. Cancer Ther.* **2008**, *7*, 243–251; b) D. Baum, S. Silverman, *Cell. Mol. Life Sci.* **2008**, *65*, 2156–2174; c) M. J. Cairns, T. M. Hopkins, C. Witherington, L. Wang, L. Q. Sun, *Nat. Biotechnol.* **1999**, *17*, 480–486.
[8] a) M. J. Cairns, A. King, L. Q. Sun, *Nucleic Acids Res.* **2003**, *31*, 2883–2889; b) S. Schubert, D. C. Grunert, H. Zeichhardt, V. A. Erdmann, J. Kurreck, *Nucleic Acids Res.* **2003**, *31*, 5982–5992.
[9] M. Cieslak, J. Szymanski, R. W. Adamiak, C. S. Cierniewski, *J. Biol. Chem.* **2003**, *278*, 47987–47996.
[10] a) D. Pantarotto, R. Singh, D. McCarthy, M. Erhardt, J. P. Briand, M. Prato, K. Kostarelos, A. Bianco, *Angew. Chem. Int. Ed.* **2004**, *43*, 5242–5246; *Angew. Chem.* **2004**, *116*, 5354–5358; b) K. Yehl, J. P. Joshi, B. L. Greene, R. B. Dyer, R. Nahta, K. Salaita, *ACS Nano* **2012**, *6*, 9150–9157.
[11] a) Z. Zhao, H. Fan, G. Zhou, H. Bai, H. Liang, R. Wang, X. Zhang, W. Tan, *J. Am. Chem. Soc.* **2014**, *136*, 11220–11223; b) Y. Yuan, S. Wu, F. Shu, Z. Liu, *Chem. Commun.* **2014**, *50*, 1095–1097; c) Y. Chen, D. Ye, M. Wu, H. Chen, L. Zhang, J. Shi, L. Wang, *Adv. Mater.* **2014**, *26*, 7018–7026.
[12] a) F. Chen, R. Wang, Z. Li, B. Liu, X. Wang, Y. Sun, D. Hao, J. Zhang, *Nucleic Acids Res.* **2004**, *32*, 2336–2341; b) J. C. Lam, Y. Li, *ChemBioChem* **2010**, *11*, 1710–1719.
[13] R. Deng, X. Xie, M. Vendrell, Y. Chang, X. Liu, *J. Am. Chem. Soc.* **2011**, *133*, 20168–20171.
[14] a) See Ref. [8b]; b) B. Wang, L. Cao, W. Chiuman, Y. Li, Z. Xi, *Biochemistry* **2010**, *49*, 7553–7562; c) A. Abdelgany, M. Wood, D. Beeson, *J. Gene Med.* **2007**, *9*, 727–738.
[15] a) F. S. Santiago, H. C. Lowe, M. M. Kavurma, C. N. Chesterman, A. Baker, D. G. Atkins, L. M. Khachigian, *Nat. Med.* **1999**, *5*, 1264–1269; b) R. G. Fahmy, C. R. Dass, L. Q. Sun, C. N. Chesterman, L. M. Khachigian, *Nat. Med.* **2003**, *9*, 1026–1032.

Received: November 25, 2014
Revised: January 23, 2015
Published online: February 26, 2015

